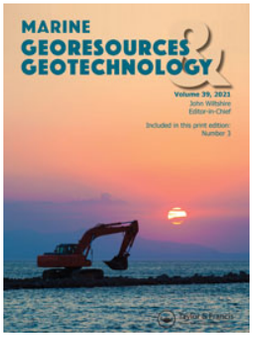

Taylor & Francis
Taylor & Francis Group

Marine Georesources & Geotechnology

ISSN: 1064-119X (Print) 1521-0618 (Online) Journal homepage: https://www.tandfonline.com/loi/umgt20

X-ray analysis on the effect of sample preparation on the microstructure of calcareous sands

Jinquan Shi, Wim Haegeman, Arjen Mascini & Veerle Cnudde

To cite this article: Jinquan Shi, Wim Haegeman, Arjen Mascini & Veerle Cnudde (2021) X-ray analysis on the effect of sample preparation on the microstructure of calcareous sands, Marine Georesources & Geotechnology, 39:3, 302-311, DOI: 10.1080/1064119X.2019.1698680

To link to this article: https://doi.org/10.1080/1064119X.2019.1698680

MARINE GEORESOURCES & GEOTECHNOLOGY
2021, VOL. 39, NO. 3, 302–311
https://doi.org/10.1080/1064119X.2019.1698680

X-ray analysis on the effect of sample preparation on the microstructure of calcareous sands

Jinquan Shi[a], Wim Haegeman[a], Arjen Mascini[b] and Veerle Cnudde[b,c]

[a]Department of Civil Engineering, Ghent University, Technologiepark 68, Zwijnaarde, B-9052, Belgium; [b]Department of Geology, Ghent University, Proeftuinstraat 86, Ghent, B-9000, Belgium; [c]Department of Earth Sciences, Utrecht University, Princetonlaan 8a, Utrecht, 3584 CB, The Netherlands

ABSTRACT

The behavior of a sandy soil in laboratory tests is highly influenced by the sedimentation technique. In this study, a calcareous sand from the reclamation site in Persian Gulf is used as the material to reconstruct laboratory scale samples with the air and water pluviation, moist and dry tamping and dry funnel deposition methods. The microstructure of these calcareous sand samples, including the homogeneity and the spatial consistency of the fabric anisotropy, is examined using X-ray tomography. It is shown that the sample preparation method introduces distinct differences in the sample uniformity and the spatial fabric anisotropy. The sample density varies along the sample height and is highly affected by the boundary effect. The fabric anisotropy is proved to have spatial consistency except for the sample made by the water pluviation method. In the water pluviation sample, the boundary effect on the fabric anisotropy is significant, which is explained by the grain-water interaction during the sedimentation.

ARTICLE HISTORY
Received 7 July 2019
Accepted 23 October 2019

KEYWORDS
Sediments; sample preparation method; fabric anisotropy; x-ray tomography

1. Introduction

The sample reconstitution techniques for sandy soils in laboratory tests have been widely studied during the last decades. Efforts are mainly paid on the imitation of the soil deposition in both natural (sedimentation, alluviation) and artificial (hydraulic reclamation, vibrocompaction) states due to the difficulty of obtaining undisturbed samples from the site (Mulilis et al., 1977; Vaid et al., 1999; Ghionna and Porcino, 2006; Chang et al., 2011). For example, Ghionna and Porcino (2006) showed that for a coarse silica sand, the samples reconstituted by water sedimentation exhibit similar liquefaction resistance with the undisturbed samples. In earlier study conducted by Mulilis et al. (1977) on Monterey No.0 sand, samples made by moist tamping and moist vibratory compaction methods exhibit similar dynamic strength with the undisturbed samples.

For granular soils, pluviation, tamping and vibration are most frequently used for the sample reconstitution in laboratory. The deposition environment, referring to dry and wet states, also plays an important role in the fabric formation. Many studies, such as Miura and Toki (1982), Lagioia et al. (2006), Thomson and Wong (2008), Sadrekarimi and Olson (2012) and Li et al. (2018), have shown that the sample preparation method introduces significant variation in soil fabric and further leads to different mechanical responses within small to medium strain ranges. Mostly, the microstructure analysis on the sandy soils focuses on the homogeneity and the fabric anisotropy. Vaid and Negussey (1988) and Selig and Ladd (1978) indicated that the fabric inhomogeneity reduces the liquefaction resistance of sand samples. Many studies, such as Sze and Yang (2014) and Escribano and Nash (2015), reported that the stiffness anisotropy and the liquefaction resistance of sand samples vary with the fabric anisotropy. To check the homogeneity, the common way is to solidify the sample with gelatin or resin and then intersected segments with equal length are weighted to determine the overall void ratio (Vaid and Negussey, 1988). Recent studies show that two techniques, SEM (Scanning Electron Microscope) and X-ray tomography, are also able to investigate the microstructures of the laboratory geomaterial samples. For example, with the SEM method, Yang et al. (2008) compared the particle orientations in samples made by moist tamping and dry pluviation methods and they found that the fabric of the moist tamping sample is more isotropic. Similar conclusions are also given by Kodicherla et al. (2018). Thomson and Wong (2008) used medical CT equipment to analyze the void ratio redistribution in the water pluviated and moist tamped specimens during undrained shearing. During the last decades, micro-CT techniques have been developed and introduced to investigate the micro structure of geomaterials (Oda et al., 2004; Cnudde et al., 2006; Fonseca et al., 2012; Cnudde and Boone, 2013; Higo et al., 2013; Alikarami et al., 2015; De Boever et al., 2015; Bultreys et al., 2016). Sun et al. (2019) used X-ray tomography to investigate the fabric anisotropy of the air pluviation samples and they found that the particle long axes and the contact normals prefer

CONTACT Jinquan Shi jinquan.shi@ugent.be Department of Civil Engineering, Ghent University, Technologiepark 68, B-9052 Zwijnaarde, Belgium

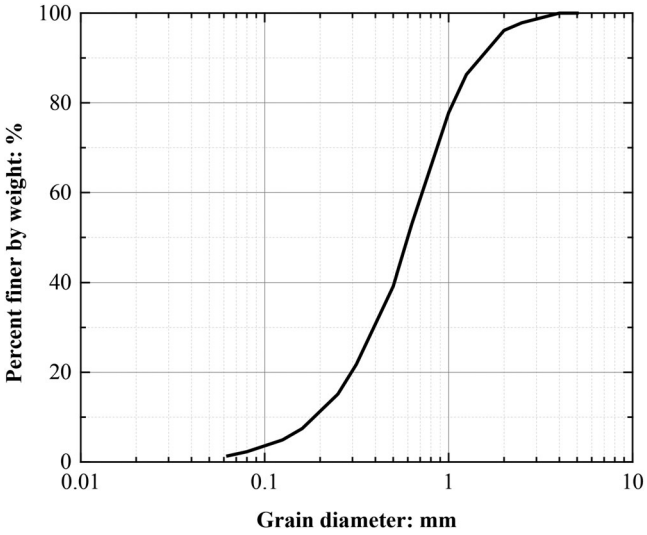

Figure. 1. Particle size gradation of S1 sand.

horizontal and vertical alignments respectively. Compared with SEM, X-ray tomography provides a nondestructive technique for inspecting the internal microstructure of soil samples and achieving the fabric examination in 3 dimensions. However, the spatial resolution of most micro-CT scanners stays at micron level, which is lower than the nanometer level of SEM (De Haan et al., 2019; Du Plessis et al., 2017). In addition, samples need to be placed as close as possible to the X-ray source in cone beam type micro CT systems, while keeping the full sample in view. Therefore, the sample diameter typically limits the maximum achievable resolution and image volume for this imaging technique. In order to obtain the high spatial resolution, some studies conduct scan tests on cores extracted from an entire sample (Higo et al., 2013). Recently, a new testing apparatus was fabricated to fit the samples in the reduced scale for the micro CT scan, as reported by Hall et al. (2010) and Zhao et al. (2019).

In this study, a calcareous sand, named S1 sand, used as the hydraulic fill material for the offshore land reclamation in the Persian Gulf, is selected as the testing material. Studies, such as Van Impe et al. (2015), Wils et al. (2015) and Ha Giang et al. (2017), performed a series of laboratory tests on this calcareous sand to address its mechanical behavior for the practical engineering application. However, the sample preparation method is not taken into account in their studies. Van Impe et al. (2015) concluded that it is difficult to evaluate the quality of the reclamation based on data correlation between laboratory and in situ tests. They attributed the difficulty to several factors varying in laboratory and in situ testing like stress history, reclamation method and particle crushing. So, the effect of sample preparation method in the laboratory test should not be neglected.

To sum up, the aim of this study is to examine the homogeneity and the fabric anisotropy of the calcareous samples on a laboratory scale by using micro CT tomography. Five methods including air and water pluviation, dry and moist tamping and dry funnel deposition are selected as the sample reconstitution techniques. The spatial consistency of the fabric anisotropy within each sample is examined, which is seldom reported in previous studies.

2. Test material and sample preparation

The physical properties of S1 sand are: a specific gravity $G_s = 2.81$; a mean grain diameter $D_{50} = 0.602$ mm; a coefficient of uniformity $C_u = 3.89$; a maximum void ratio $e_{max} = 1.19$; a minimum void ratio $e_{min} = 0.73$. The content of $CaCO_3$ of S1 sand is over 95% due to its composition mainly consisting of shell and coral. The particle size gradation is shown in Figure 1.

In order to make the samples in the laboratory scale, all the samples are prepared in a Perspex mold having an inner diameter of 50 mm and height of 120 mm. The air pluviation method is carried out with a self-designed pluviator containing 5 layers of sieves and a funnel having an adjustable opening controlling the sample density. In the water pluviation method, the mold is first half filled with water then sands are poured through a pluviator having sieves and the same diameter as the mold. The air and water pluviation devices are illustrated in Figure 2. The initial density in the water pluviation sample is very loose. Therefore, a densification is carried out by tamping the mold side with a hammer. In the dry and moist tamping method, samples are prepared in 5 layers and 10 layers respectively. The undercompaction method is used to control the homogeneity (Selig and Ladd, 1978). For the moist tamping method, sands mixed with water 5% by mass are prepared 24 hours before the reconstruction. The dry funnel deposition sample is prepared with a long neck funnel elevated slowly to keep the opening zero height to the sample surface constant. Then the vibration by tapping the mold side is applied to achieve the target density. In this study, the in-situ density of the reclamation area of 60% is targeted (Van Impe et al., 2015).

3. X-ray tomography

The micro CT scanner used in the present study, named HECTOR, is developed in the X-ray tomography Centre of the Ghent University (UGCT). Further details on the scanner can be found in (Masschaele et al., 2013). The system consists of three principal components which are the high power X-ray flux source, a rotation stage table and the flat panel detector, as shown in Figure 3. Here, an accelerating voltage of 160 kV at 25 W is used to acquire 2401 projections per image with an exposure time of 1000 ms per projection. The full 120 mm length of the samples is imaged by stacking three images together to form one image with a high aspect ratio. The obtained reconstructed voxel size was 28 μm for all images.

The image processing is conducted with Octopus Analysis (Vlassenbroeck et al., 2007) . Firstly, the 3 D volume is stacked by a group of horizontal slices reconstructed from the X-ray radiographs. Then the vertical slices are sectioned from the 3 D volume in X and Y directions respectively, as illustrated in Figure 4. In this study, due to the large laboratory sample scale and the resolution coordination for the well graded sands, the

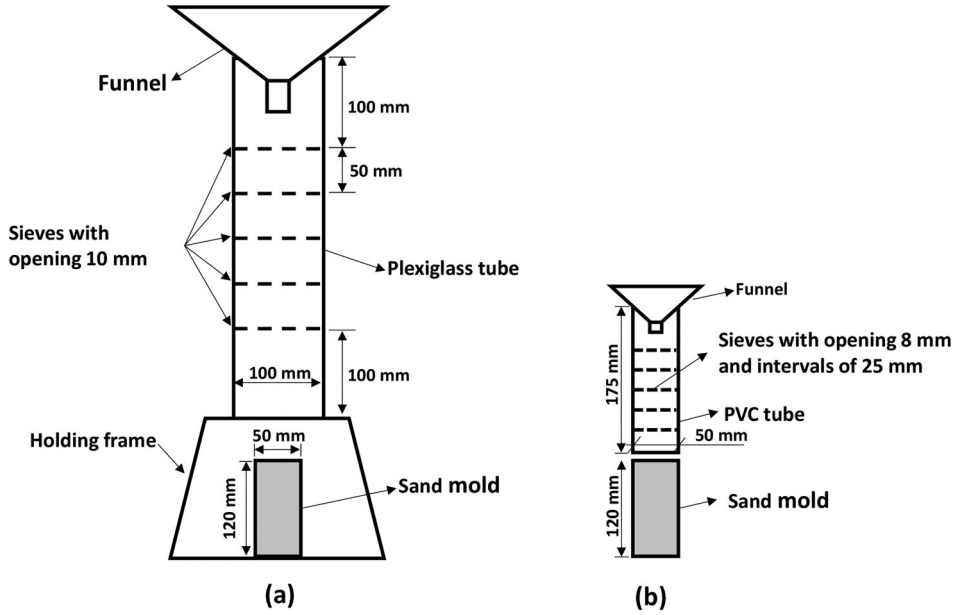

Figure 2. Diagram of the pluviation devices: (a) air pluviation; (b) water pluviation.

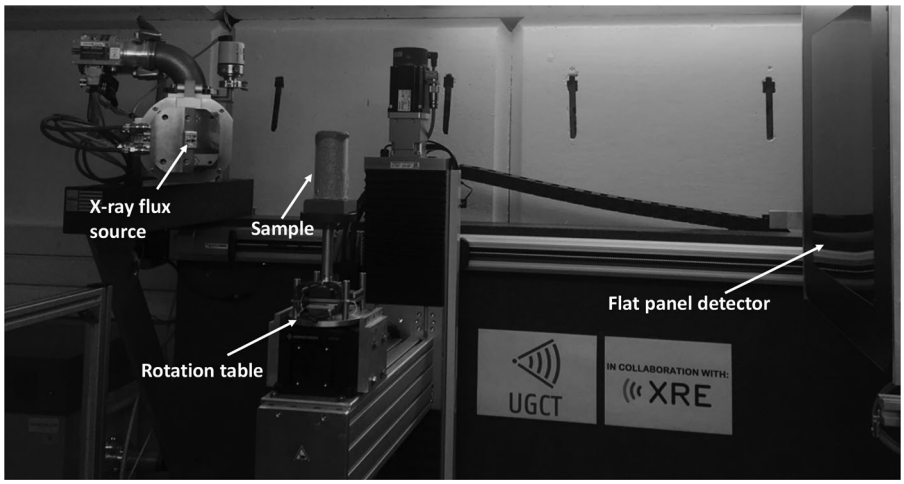

Figure 3. The X-ray CT apparatus "HECTOR" at UGCT.

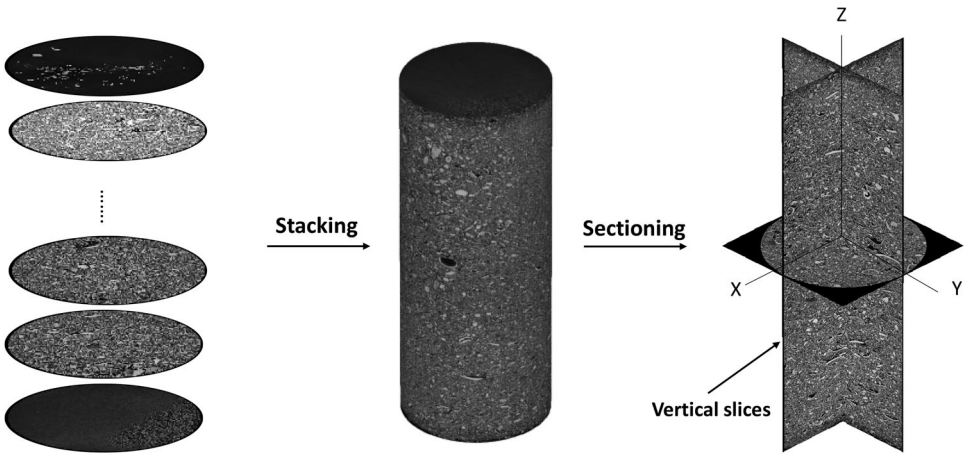

Figure 4. 3 D volume reconstruction and slices sectioning of the air pluviation sample with Octopus Analysis.

resolution of the scans increases to 28 μm (voxel size unit), meaning that measuring the real porosity becomes unattainable. However, the aim of this study is to evaluate the homogeneity and the real porosity is replaceable by another parameter as long as the density on each slice is quantified based on the same criterion. By assuming that the chemical

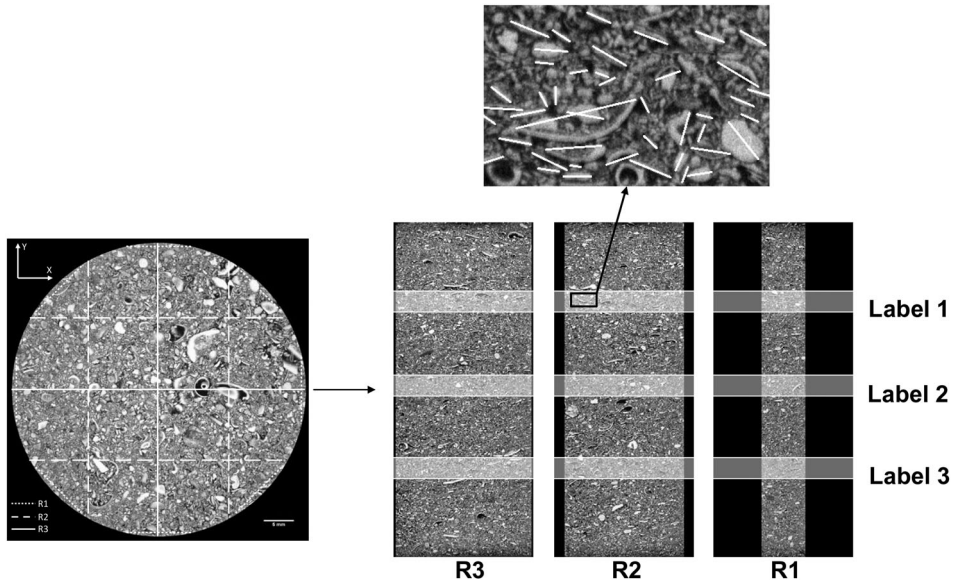

Figure 5. Image preparation for particle orientation analysis: labelling the long axis of grains on the vertical slices in the sample made by air pluviation.

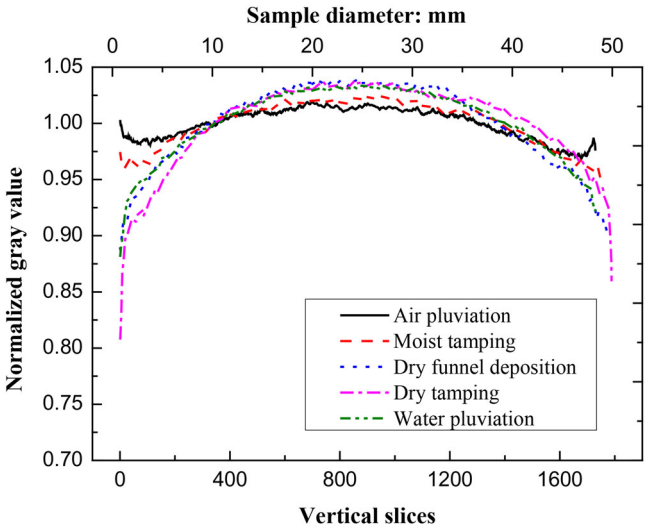

Figure 6. Radial homogeneity evaluated by the normalized gray value.

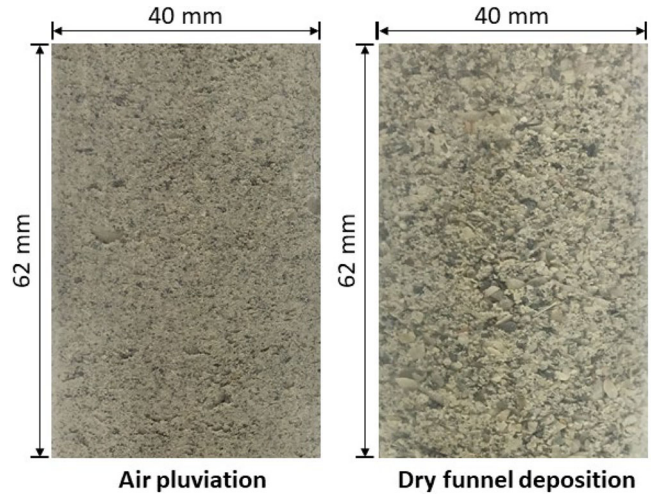

Figure 7. Side views of the air pluviation and dry funnel deposition samples

and mineralogical composition of the S1 sands are the same for all the samples, the average gray value per slice can be used as a metric for the local density of the grain packing. The average gray value per slice reflects both the grain composition as well as the porosity. The higher the average gray value, the higher the average atomic number of the mineral phases present in that slice and the higher density. In this study, the gray value of each slice is given directly by the Octopus Analysis so the spatial uniformity of the five samples can be determined.

In order to quantify the fabric anisotropy, the particle orientation is measured from the clockwise angle between the grain principle axis and the horizontal line. Three horizontal labels located equally along the height are labeled on the vertical slices, R1, R2 and R3 sectioned at different positions along the diameter in two orthogonal planes, as shown in Figure 5. Grains on these labels are marked manually for measuring the particle orientation. Finally, the spatial consistency of the fabric anisotropy in the radial and vertical directions is examined. Yang et al., (2008) found that the horizontal slice is transverse isotropy and the fabric anisotropy is insignificant. Therefore, in this study, only the grains on the vertical slices are taken into account. As explained, the particle orientation is evaluated for grains of which the diameters are minimum of 3 to 5 voxels. The grain contact normal is also a parameter indicating anisotropy. Kodicherla et al. (2018) mentioned that the fabric tensor inferred from the grain contact normal orientation is used to describe the stress induced anisotropy. However, in this study, the limited image resolution is not sufficient for quantifying the grain contact, so analysis on the contact normal orientation is not considered.

4. Test results

4.1. Sample uniformity

The gray values measured on the vertical and horizontal slices are normalized by their averaged values respectively so

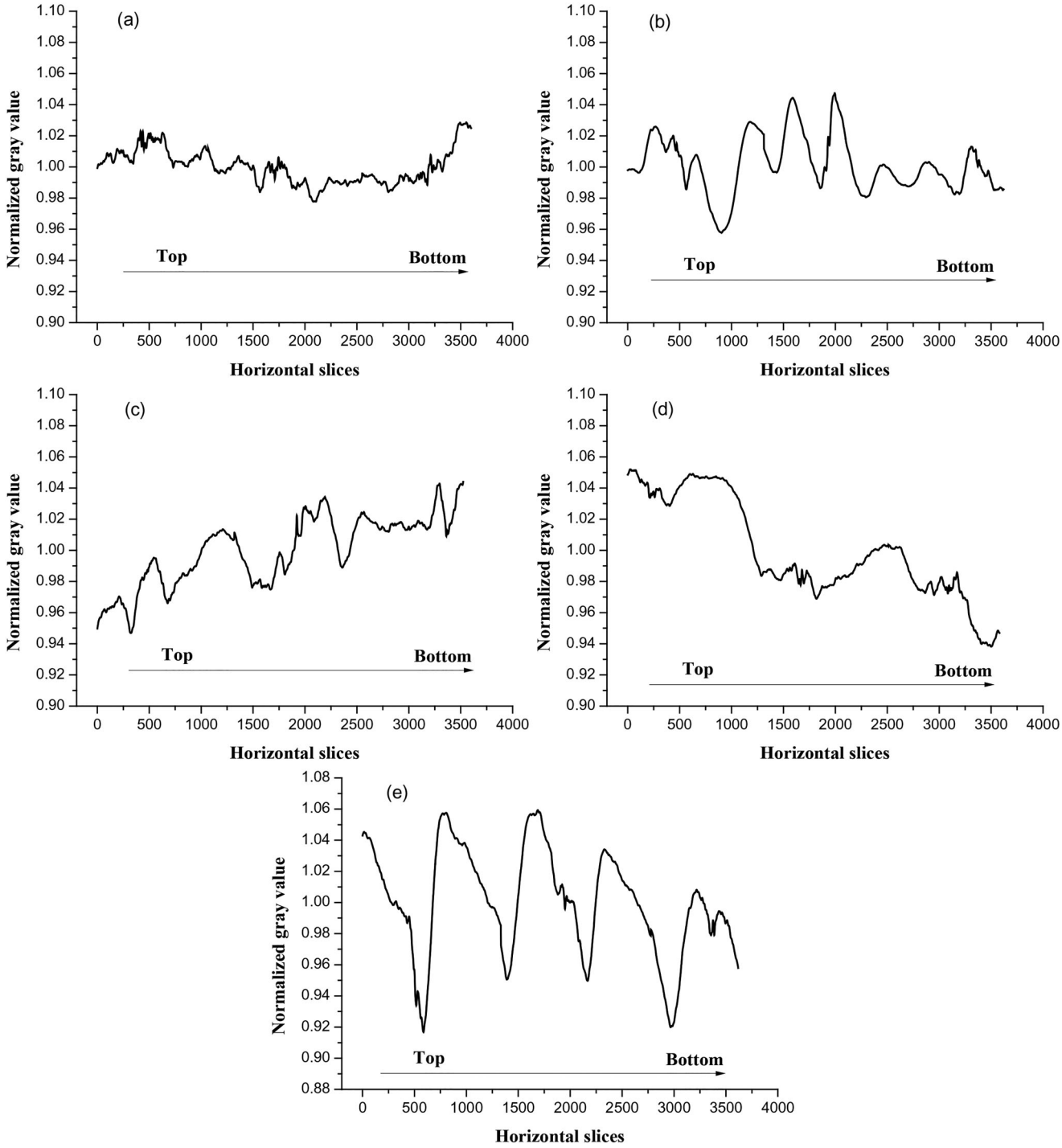

Figure 8. The density variation along the sample height: (a) air pluviation; (b) moist tamping; (c) dry funnel deposition; (d) water pluviation; and (e) dry tamping.

the density variation along the height and in the radial direction is obtained. Figure 6 presents the radial homogeneity for the samples prepared by the five methods. It is seen that for all samples, the density decreases with the increase of the distance from the central axis. Similar conclusions are also reported by Marketos and Bolton (2009) and Camenen et al. (2013) that zones close to the sample boundary have higher porosity. However, in this study, it is also noteworthy that this nonuniformity varies with the sample preparation method. The variation of the radial density in the air pluviation sample is 2%, which is the slightest. The most significant variation is observed in the dry tamping sample, corresponding to a density reduction of 17% at the boundary. For the water pluviation and the dry funnel deposition samples, the radial density variation is around 11% which is lower than that of the dry tamping sample. A variation of around 5% is observed in the moist tamping sample. In the zones close to the central axis, water pluviation, dry tamping and dry funnel deposition samples show an identical density deviation from the mean. The variation of the air pluviation sample is still the least and slightly higher than that of the moist tamping sample. In addition, it is interesting to note that there is a sudden density increase at the position very close to the boundary in the air pluviation sample. From the

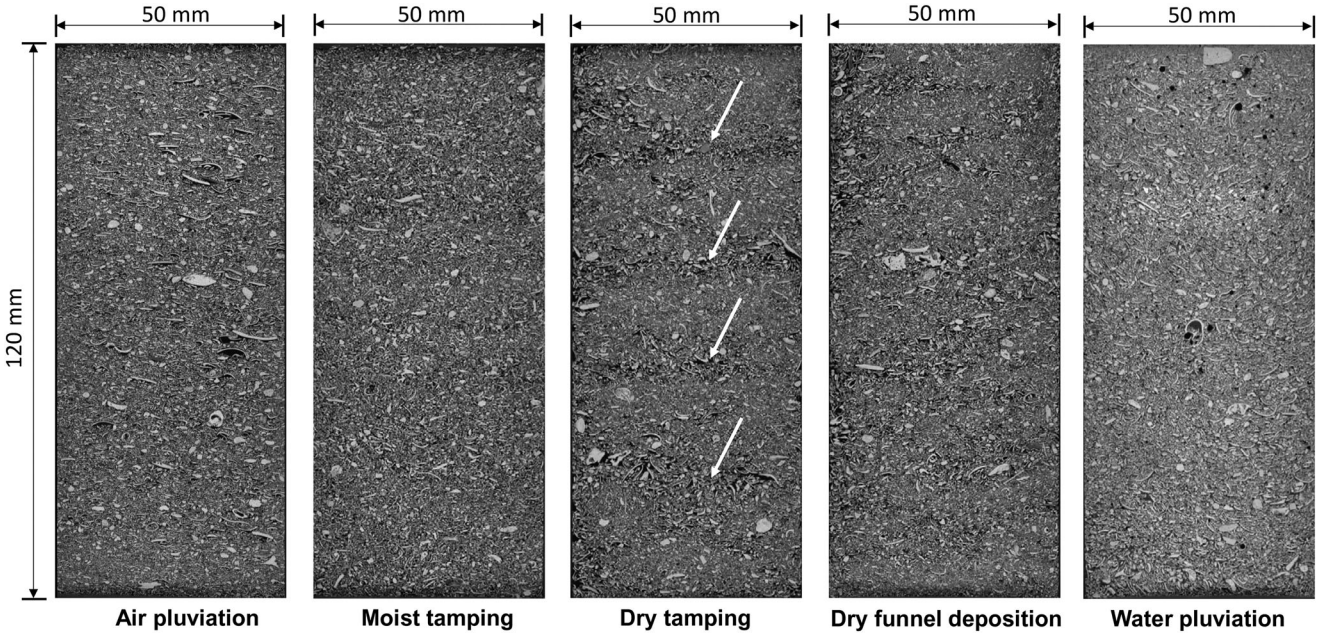

Figure 9. Central vertical slices of the samples made by the five methods: visible interfacial faces between layers in the dry tamping sample.

direct observation on the scanned samples, it is seen that finer grains concentrate at the boundary of the air pluviation sample resulting in an increase of the density. This is clearly distinct from the other samples. For example, Figure 7 shows the comparison of the side views of the air pluviation and the dry funnel deposition samples.

Looking to the density variation along the sample height, samples prepared by different methods also show distinct disparity, as exhibited in Figure 8. The sample made by the air pluviation method shows the slightest fluctuation among the five samples. It is seen that the density variation is significant in the samples prepared by layers such as tamping and dry funnel deposition. However, the fluctuation in the moist tamping sample is smaller and the density is almost the same at the top and bottom. It is deemed the tamping number required to reach the targeted density increases hugely in the moist tamping sample due to the high capillary force and the tamping faces between layers are compacted more tightly, reducing the density variation. Figure 9 shows the microscopic interfacial faces between layers in the dry tamping sample, which are not observed in the samples prepared by the other methods. In the dry funnel deposition sample, a higher density at the sample bottom is observed. A similar conclusion is also given by Flitti et al. (2019) from the X-ray scan tests conducted on a silica sand. Vaid and Negussey (1988) reported that the vibration applied for the densification may cause a looser state in the top zone if an improper seating load is applied on the sample surface. Although a seating weight is used in this study, it is seen the density heterogeneity along the sample height is not avoided.

In the water pluviation sample, however, a lower density is observed at the sample bottom, which is opposite to the finding in the dry funnel deposition sample. Figure 10 shows two horizontal slices from the top and bottom of the sample respectively. It is seen that the gray value, circled in layer 889 and representing small grains, is rare in the layer 3863. Vaid and Negussey (1988) showed that the water pluviation is a repeatable method to produce a uniform sample. In this study, the nonuniformity is ascribed to the used sand having a different gradation. The water in the mold moves up during the sand deposition, creating an uplift force acting on the sand grains. Therefore, the grains small in diameter deposit slowly or even move upward inversely. Compared with the uniform sand used by Vaid and Negussey (1988), the sand in this study is well graded and therefore the segregation of grains after deposition is more pronounced, resulting in the nonuniformity in density along the sample height. In the study of Flitti et al. (2019), an opposite conclusion about the uniformity in the water pluviation sample is reported, showing a higher density at the sample bottom. The difference can again partly be attributed to the sand gradation since they use a more uniform sand so the particle segregation is reduced. In addition, they deposit sands in several layers with a long neck funnel and the densification depends on tamping. Therefore, the disturbance from water flow is reduced and the grain segregation is further decreased. Also, the tamping technique can lead to the higher density at the lower layers.

4.2. Fabric anisotropy

In order to verify if the number of the particles selected is high enough, an examination on the particle orientation distribution of groups containing different number of grains is carried out. The particles are randomly selected from the vertical central slice in the air pluviation sample and the results are shown in Figure 11. It is seen that the differences between the lines become insignificant if the number of the particles is greater than 1000. Therefore, a horizontal label with 4 mm in height, containing sufficient grains, is finally selected. The number of grains used in the different labels is listed in Table 1.

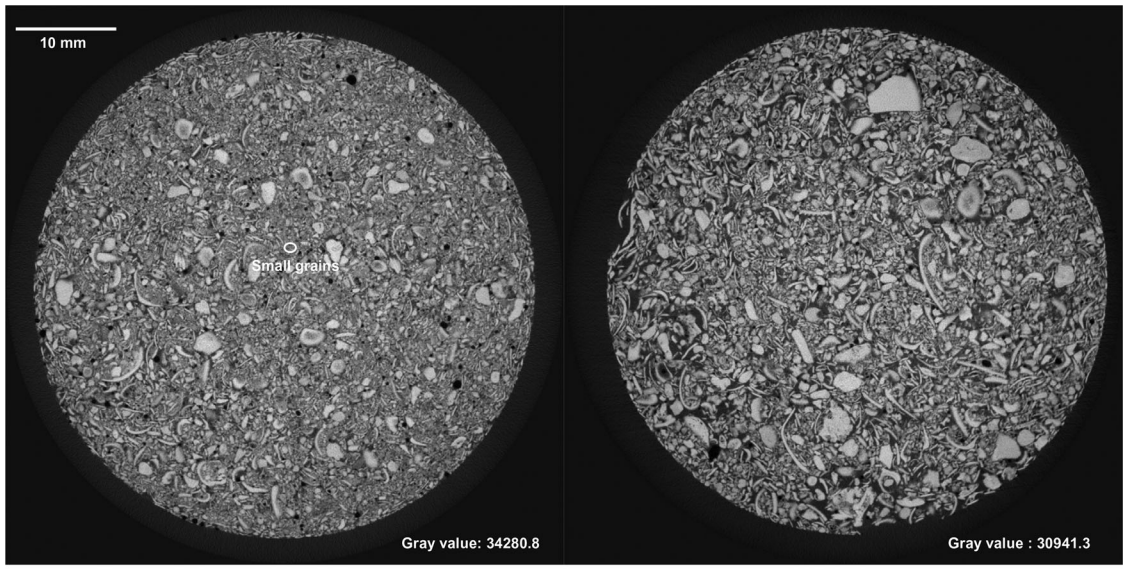

Figure 10. Heterogeneity of density at the top (left) and bottom (right) of the water pluviation sample.

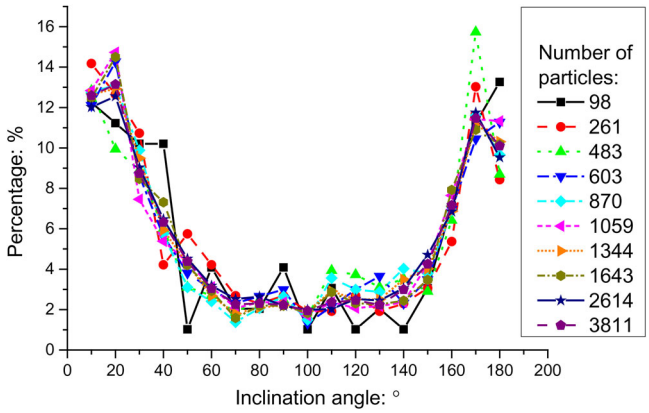

Figure 11. Verification of the amount of the analyzed grains.

Figure 12 shows the particle orientation distribution of the grains in the above mentioned three horizontal labels of the samples prepared by the five methods. So, the variation of the particle orientation across the sample height is indicated since the three labels are located at different heights. It is seen that the particle orientation exhibits a similar distribution on the three labels for each preparation method, indicating that the fabric anisotropy is consistent in the vertical direction and the effect of sample preparation method on the fabric anisotropy distribution along the sample height can be neglected. In addition, combined with the results of uniformity, it is also noted that although the samples have a vertical density variation, the fabric anisotropy is unaffected.

Similarly, the particle orientation distribution along the diameter is drawn in Figure 13. It is shown that except for the water pluviation sample, the angle distribution at the three locations exhibits high consistency. In the water pluviation sample, the grains close to the boundary tend to be vertically aligned. Figure 14 shows a capture from the central section across the diameter in the water pluviation sample. It is seen that the particle orientation varies with the

Table 1. The particle number for quantifying anisotropy distribution.

	Particle number					
Samples	Label 1	Label 2	Label 3	R1	R2	R3
Air pluviation	1161	1474	1613	1340	1804	1104
Moist tamping	2047	1916	1815	1614	2538	1626
Dry funnel deposition	2269	2520	2609	1683	3559	2116
Dry tamping	2168	1925	1913	1614	2786	1606
Water pluviation	1298	1599	1503	1263	1967	1170

distance to the central axis and shows an axisymmetrical distribution. This particle alignment can again be attributed to the effect of water flow on the movement of the sand grains during deposition. Figure 15 shows the trajectory of sand and water flow during the construction of the water pluviation sample. Although the deposition area of the sand once passed the sieves becomes wider, it is still smaller than the mold opening. So, less deposition intensity in the peripheral area provides the escape space for the water pushed by the falling sands. Therefore, a stronger upward force is applied to the sand grains at the boundary, leading to the inclined deposition angles. The closer to the sample boundary, the more vertical the particle orientation becomes. This variation of the radial fabric anisotropy indicates that only the grains on the vertical central slices can represent the overall fabric anisotropy in the water pluviation sample due to its central symmetry geometry.

5. Conclusions

The uniformity and the spatial consistency of the fabric anisotropy in the calcareous sand samples prepared by the air and water pluviation, moist and dry tamping and dry funnel deposition methods are evaluated using X-ray tomography. For the uniformity, it is concluded that the zones close to the sample boundary show lower densities for all the preparation methods. The air pluviation and dry tamping samples are respectively the least and the most affected

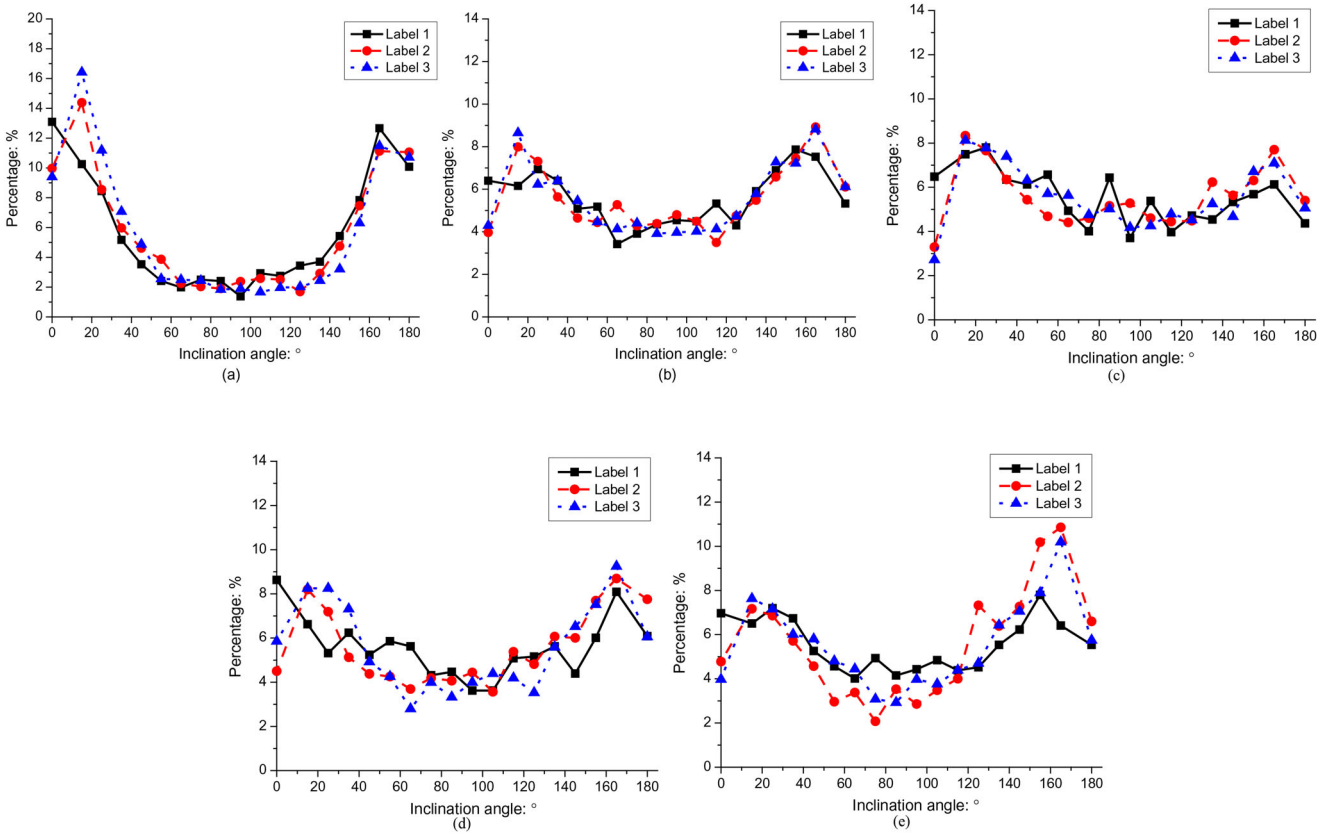

Figure 12. Particle orientation distribution at different heights: (a) air pluviation; (b) moist tamping; (c) dry funnel deposition; (d) water pluviation; and (e) dry tamping.

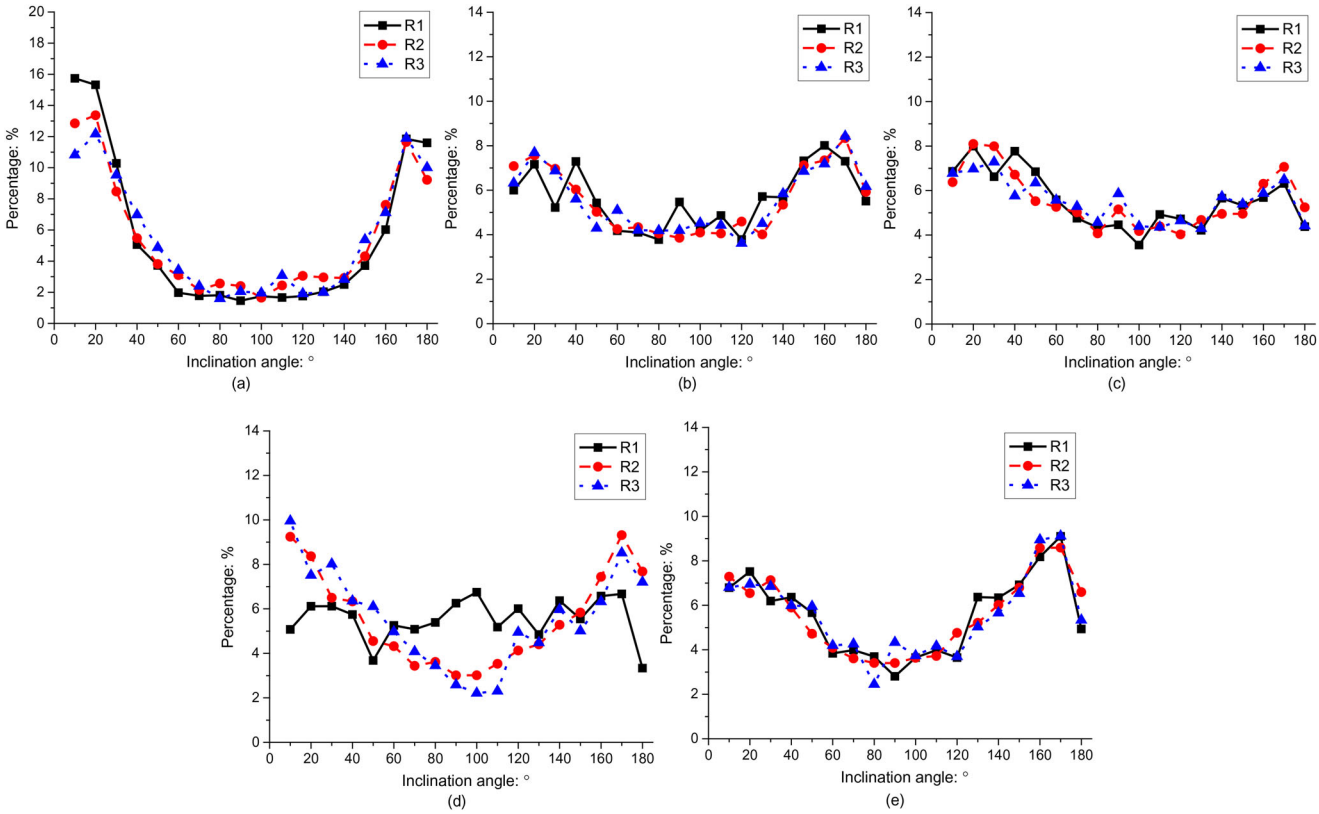

Figure 13. Particle orientation distribution at different radial positions: (a) air pluviation; (b) moist tamping; (c) dry funnel deposition; (d) water pluviation; and (e) dry tamping.

Figure 14. Capture from the central section in the water pluviation sample.

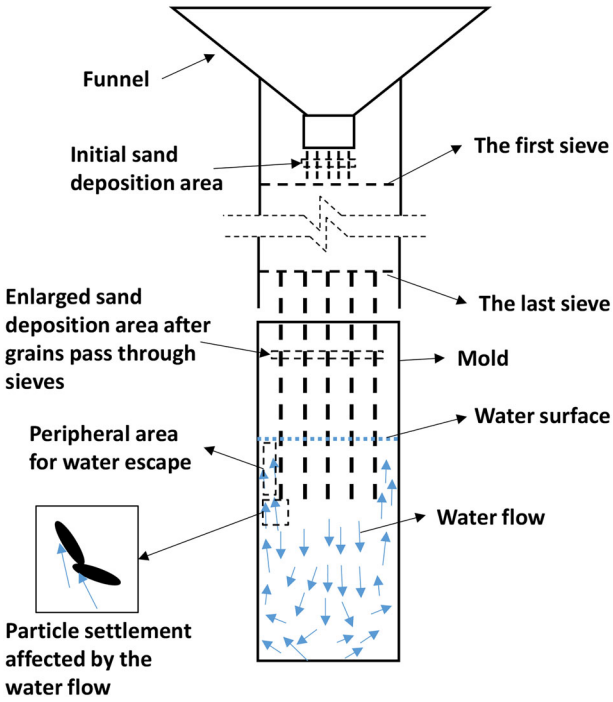

Figure 15. The trajectory of sands and water flow during the reconstruction of the water pluviation sample.

by the boundary. Along the height, the sample prepared by the air pluviation method shows the highest homogeneity. The density decreases and increases from the top to the bottom for the water pluviation and dry funnel deposition samples respectively. The density in the samples prepared in layers shows variation along the sample height and the fluctuation is the most significant in the dry tamping sample. The fabric anisotropy distributes uniformly along the sample height for all preparation methods. Due to the water flow in the deposition process, the water pluviation is the only method producing a sample without radial consistency in fabric anisotropy.

Acknowledgements

The authors would like to acknowledge the Centre for X-ray Tomography at Ghent University, Belgium, for allowing the performance of the experiments. The Ghent University Special Research Fund (BOF-UGent) is acknowledged for the financial support to the BOF.EXP.2017.0007.

Disclosure statement

No potential conflict of interest was reported by the author(s).

Funding

The first author acknowledges the financial support from the China Scholarship Council (No. 201607040079).

ORCID

Jinquan Shi http://orcid.org/0000-0003-1700-9127

References

Alikarami, R., E. Andò, M. Gkiousas-Kapnisis, A. Torabi, and G. Viggiani. 2015. Strain Localisation and Grain Breakage in Sand under Shearing at High Mean Stress: Insights from in Situ X-Ray Tomography. *Acta Geotechnica* 10 (1):15–30. doi:10.1007/s11440-014-0364-6.

Bultreys, T., W. De Boever, and V. Cnudde. 2016. Imaging and Image-Based Fluid Transport Modeling at the Pore Scale in Geological Materials: A Practical Introduction to the Current State-of-the-Art. *Earth-Science Reviews* 155:93–128. doi:10.1016/j.earscirev.2016.02.001.

Camenen, J. F., I. Cavarretta, S. Hamlin, and E. Ibraim. 2013. Experimental and Numerical Assessment of a Cubical Sample Produced by Pluviation. *Géotechnique Letters* 3 (2):44–51. doi:10.1680/geolett.13.00028.

Chang, N., G. Heymann, and C. Clayton. 2011. The Effect of Fabric on the Behaviour of Gold Tailings. *Géotechnique* 61 (3):187–197. doi:10.1680/geot.9.P.066.

Cnudde, V., and M. N. Boone. 2013. High-Resolution X-Ray Computed Tomography in Geosciences: A Review of the Current Technology and Applications. *Earth-Science Reviews* 123:1–17. doi:10.1016/j.earscirev.2013.04.003.

Cnudde, V., B. Masschaele, M. Dierick, J. Vlassenbroeck, L. V. Hoorebeke, and P. Jacobs. 2006. Recent Progress in X-Ray CT as a Geosciences Tool. *Applied Geochemistry* 21 (5):826–832. doi:10.1016/j.apgeochem.2006.02.010.

De Haan, K., Z. S. Ballard, Y. Rivenson, Y. Wu, and A. Ozcan. 2019. Resolution Enhancement in Scanning Electron Microscopy Using Deep Learning. *arXiv* preprint arXiv:1901.11094.

De Boever, W., H. Derluyn, D. Van Loo, L. Van Hoorebeke, and V. Cnudde. 2015. Data-Fusion of High Resolution X-Ray CT, SEM and EDS for 3D and Pseudo-3D Chemical and Structural Characterization of Sandstone. *Micron* 74:15–12. doi:10.1016/j.micron.2015.04.003.

Du Plessis, A., C. Broeckhoven, A. Guelpa, and S. G. Le Roux. 2017. Laboratory X-Ray Micro-Computed Tomography: A User Guideline for Biological Samples. *Gigascience* 6 (6):1–11. doi:10.1093/gigascience/gix027.

Escribano, D. E., and D. F. T. Nash. 2015. Changing Anisotropy of G_0 in Hostun Sand during Drained Monotonic and Cyclic Loading. *Soils and Foundations* 55 (5):974–984. Elsevier, doi:10.1016/j.sandf.2015.09.004.

Flitti, A., N. Della, T. De Kock, V. Cnudde, and R. D. Verástegui-Flores. 2019. Effect of Initial Fabric on the Undrained Response of Clean Chlef Sand. *European Journal of Environmental and Civil Engineering*, 1–16. doi:10.1080/19648189.2019.1631217.

Fonseca, J., C. O'Sullivan, M. R. Coop, and P. D. Lee. 2012. Non-Invasive Characterization of Particle Morphology of Natural Sands. *Soils and Foundations* 52 (4):712. doi:10.1016/j.sandf.2012.07.011.

Ghionna, V. N., and D. Porcino. 2006. Liquefaction Resistance of Undisturbed and Reconstituted Samples of a Natural Coarse Sand from Undrained Cyclic Triaxial Tests. *Journal of Geotechnical and Geoenvironmental Engineering* 132 (2):194–202. doi:10.1061/(ASCE)1090-0241(2006)132:2(194).

Ha Giang, P. H., P. O. Van Impe, W. F. Van Impe, P. Menge, and W. Haegeman. 2017. Small-Strain Shear Modulus of Calcareous Sand and Its Dependence on Particle Characteristics and Gradation. *Soil*

Dynamics and Earthquake Engineering 100:371–379. doi:10.1016/j.soildyn.2017.06.016.

Hall, S. A., M. Bornert, J. Desrues, Y. Pannier, N. Lenoir, G. Viggiani, P. BéSUELLE., et al. 2010. Discrete and Continuum Analysis of Localised Deformation in Sand Using X-Ray μCT and Volumetric Digital Image Correlation. *Géotechnique* 60 (5):315–322. doi:10.1680/geot.2010.60.5.315.

Higo, Y., F. Oka, T. Sato, Y. Matsushima, and S. Kimoto. 2013. Investigation of Localized Deformation in Partially Saturated Sand under Triaxial Compression Using Microfocus X-Ray CT with Digital Image Correlation. *Soils and Foundations* 53 (2):181–198. Elsevier, doi:10.1016/j.sandf.2013.02.001.

Kodicherla, S. P. K., G. Gong, L. Fan, C. K. S. Moy, and J. He. 2018. Effects of Preparation Methods on Inherent Fabric Anisotropy and Packing Density of Reconstituted Sand. *Cogent Engineering* 5 (1): 1533363. doi:10.1080/23311916.2018.1533363.

Lagioia, R., A. Sanzeni, and F. Colleselli. 2006. Air, Water and Vacuum Pluviation of Sand Specimens for Triaxial Apparatus. *Soils and Foundations* 46 (1):61–67. doi:10.3208/sandf.46.61.

Li, Y., Y. Yang, H.-S. Yu, and G. Roberts. 2018. Effect of Sample Reconstitution Methods on the Behaviors of Granular Materials under Shearing. *Journal of Testing and Evaluation* 46 (6):20170126. doi:10.1520/JTE20170126.

Marketos, G., and M. D. Bolton. 2009. Flat Boundaries and Their Effect on Sand Testing. *International Journal for Numerical and Analytical Methods in Geomechanics* 32(2007), doi:10.1002/nag.835.

Masschaele, B., M. Dierick, D. Van Loo, M. N. Boone, L. Brabant, E. Pauwels, V. Cnudde, and L. Van Hoorebeke. 2013. HECTOR: A 240kV micro-CT setup optimized for research. *Journal of Physics: Conference Series*. 463 (1): 012012. doi:10.1088/1742-6596/463/1/012012.

Miura, S., and S. Toki. 1982. A Sample Preparation Method and Its Effect on Static and Cyclic Deformation-Strength Properties of Sand. *Soils and Foundations* 22 (1):61–77. doi:10.3208/sandf1972.22.61.

Mulilis, J. P., K. Arulanandan, J. K. Mitchell, C. K. Chan, and H. B. Seed. 1977. Effects of Sample Preparation on Sand Liquefaction. *Journal of the Geotechnical Engineering Division. ASCE* 103 (2): 91–108.

Oda, M., T. Takemura, and M. Takahashi. 2004. Microstructure in Shear Band Observed by Microfocus X-Ray Computed Tomography. *Géotechnique* 54 (8):539–542. doi:10.1680/geot.2004.54.8.539.

Sadrekarimi, A., and S. M. Olson. 2012. Effect of Sample-Preparation Method on Critical-State Behavior of Sands. *Geotechnical Testing Journal* 35 (4):104317–104562. doi:10.1520/GTJ104317.

Selig, E., and R. Ladd. 1978. Preparing Test Specimens Using Undercompaction. *Geotechnical Testing Journal* 1 (1):16. doi:10.1520/GTJ10364J.

Sun, Q., J. Zheng, H. He, and Z. Li. 2019. Particulate Material Fabric Characterization from Volumetric Images by Computational Geometry. *Powder Technology* 344:804–813. doi:10.1016/j.powtec.2018.12.070.

Sze, H. Y., and J. Yang. 2014. Failure Modes of Sand in Undrained Cyclic Loading: impact of Sample Preparation. *Journal of Geotechnical and Geoenvironmental Engineering* 140 (1):152–169. doi:10.1061/(ASCE)GT.1943-5606.0000971.

Thomson, P. R., and R. C. K. Wong. 2008. Specimen Nonuniformities in Water-Pluviated and Moist-Tamped Sands under Undrained Triaxial Compression and Extension. *Canadian Geotechnical Journal* 45 (7):939–956. doi:10.1139/T08-023.

Vaid, Y. P., and D. Negussey. 1988. Preparation of reconstituted sand specimens. In *Advanced triaxial testing of soil and rock*, eds. R. T. Donaghe, R. C. Chaney, and M. L. Silver, 405–417. American Societyfor Testing and Materials, Philadelphia, Pa.: Special Technocal Publication.

Vaid, Y. P., S. Sivathayalan, and D. Stedman. 1999. Influence of Specimen-Reconstituting Method on the Undrained Response of Sand. *Geotechnical Testing Journal* 22 (3):187–195. doi:10.1520/GTJ11110J.

Van Impe, P. O., W. F. Van Impe, A. Manzotti, P. Mengé, M. Van den Broeck, and K. Vinck. 2015. Compaction Control and Related Stress-Strain Behaviour of off-Shore Land Reclamations with Calcareous Sands. *Soils and Foundations* 55 (6):1474–1486. Elsevier, doi:10.1016/j.sandf.2015.10.012.

Vlassenbroeck, J., M. Dierick, B. Masschaele, V. Cnudde, L. Van Hoorebeke, and P. Jacobs. 2007. Software Tools for Quantification of X-Ray Microtomography at the UGCT. *Nuclear Instruments and Methods in Physics Research, Section A: Accelerators, Spectrometers, Detectors and Associated Equipment* 580 (1):442–445. doi:10.1016/j.nima.2007.05.073.

Wils, L., P. O. V. Impe, and W. Haegeman. 2015. One-Dimensional Compression of a Crushable Sand in Dry and Wet Conditions. *Geomechanics from Micro to Macro* :1403–1408.

Yang, Z. X., X. S. Li, and J. Yang. 2008. Quantifying and Modelling Fabric Anisotropy of Granular Soils. *Géotechnique* 58 (4):237–248. doi:10.1680/geot.2008.58.4.237.

Zhao, B., J. Wang, E. Andò, G. Viggiani, and M. Coop. 2019. An Investigation of Particle Breakage under One-Dimensional Compression of Sand Using X-Ray Micro-Tomography. *Canadian Geotechnical Journal*, doi:10.1139/cgj-2018-0548.